Journal of Catalysis **204,** 409–419 (2001)
doi:10.1006/jcat.2001.3385, available online at http://www.idealibrary.com on IDEAL®

Selective Oxidation of *para*-Xylene to Terephthalic Acid by μ_3-Oxo-Bridged Co/Mn Cluster Complexes Encapsulated in Zeolite–Y

S. A. Chavan, D. Srinivas, and P. Ratnasamy[1]

National Chemical Laboratory, Pune-411 008, India

Received May 9, 2001; revised August 10, 2001; accepted August 10, 2001

Novel, solid catalysts of μ_3-oxo-bridged Co/Mn cluster complexes, viz., $[Co_3(O)(CH_3COO)_6(pyridine)_3]^+$, $[Mn_3(O)(CH_3COO)_6(pyridine)_3]^+$, and $CoMn_2(O)(CH_3COO)_6(pyridine)_3$ (denoted $Co_3(O)$, $Mn_3(O)$, and $CoMn_2(O)$, respectively), encapsulated in zeolite-Y oxidize selectively, *para*-xylene to terephthalic acid with dioxygen. The catalysts were prepared by the "flexible ligand synthesis" method and characterized by X-ray diffraction, thermal analysis, cyclic voltammetry, Fourier transform infrared, diffuse reflectance ultraviolet–visible, X-ray photoelectron spectroscopy, and electron paramagnetic resonance spectroscopic techniques. The various physicochemical measurements confirm the presence and structural integrity of the μ_3-oxo-bridged cluster complexes in zeolite cavities. The activity and selectivity of both the "neat" and encapsulated cluster complexes followed the order $CoMn_2(O) > Mn_3(O) > Co_3(O)$, revealing the superiority of the heteronuclear complexes. Under optimal conditions, both neat and encapsulated cluster catalysts exhibit 100% *para*-xylene conversion with >98% selectivity for terephthalic acid. It is important that the key impurity, 4-carboxybenzaldehyde, is significantly lower in abundance (than the current commercial catalysts) with one of the zeolite-encapsulated catalysts, $CoMn_2(O)$–Y. Leaching of metal ions from the solid catalyst during reaction is minimal and the catalyst could be recycled without significant loss of activity. A more facile redox behavior of Co between +2 and +3 oxidation states in $CoMn_2(O)$ (confirmed by cyclic voltammetry) is perhaps responsible for high catalytic activity.

Key Words: **encapsulated complexes in zeolite–Y; oxo-bridged Co/Mn cluster catalysts; solid catalyst for *para*-xylene oxidation; terephthalic acid; selective oxidation with dioxygen; EPR; spectroscopic studies.**

INTRODUCTION

Terephthalic acid (TA), one of the largest volume commodity chemicals, is commercially manufactured, by dioxygen oxidation of *para*-xylene (PX), in a homogeneous acetic acid (HOAc) medium, using a catalyst combination of cobalt and manganese salts and bromide ion promoter (1–5). The commercial process has been optimized to the point where typical crude TA purities of 98–99.5% are achieved in yields of 96–97 mol% based on PX feed at an oxidizer contact time of 45–90 min (6–9). However, the following improvements are desirable in the commercial process: (i) replacement of the homogeneous by a heterogeneous solid catalyst system, and (ii) reduction or elimination of 4-carboxybenzaldehyde (4-CBA) and other impurities from TA, which necessitate elaborate hydrogenation and recrystallization procedures in the manufacture of purified TA required for the polyester industry. One such method of heterogenization of homogeneous catalysts is encapsulation of active metal complexes inside the pores of zeolites or zeolitic materials (10–15). Using *in situ* electronic and electron paramagnetic resonance (EPR) spectroscopic studies, we had, earlier, identified the formation of μ_3-oxo-bridged heteronuclear Co/Mn cluster complexes (Fig. 1) in the homogeneous medium during the course of the reaction (16). These oxo-bridged cluster complexes were postulated as the active species in the selective PX oxidation reaction.

In the present study, we have, for the first time, synthesized these cluster complexes and studied their spectroscopic and catalytic properties, both in the "neat" state as well as when they are encapsulated in zeolite-Y. The solid catalysts possess activities comparable to that of the neat μ_3-oxo-bridged cluster complexes and the conventional mixture of $Co/Mn/Br^-$ salts. It is interesting that the key impurity, 4-CBA, which imparts color to TA, is lower in abundance with the solid catalysts. The probable reasons for the superior performance of these encapsulated catalysts are discussed. The advantage of the solid, encapsulated μ_3-oxo-bridged heteronuclear Co/Mn cluster complexes is that they could be recycled without significant loss of activity.

EXPERIMENTAL

Materials

$Co(CH_3COO)_2 \cdot 4H_2O$, $Mn(CH_3COO)_2 \cdot 4H_2O$, glacial CH_3COOH, pyridine, and NaBr were obtained from

[1] To whom correspondence should be addressed. Fax: (91)-020-5893355. E-mail: prs@ems.ncl.res.in.

0021-9517/01 $35.00

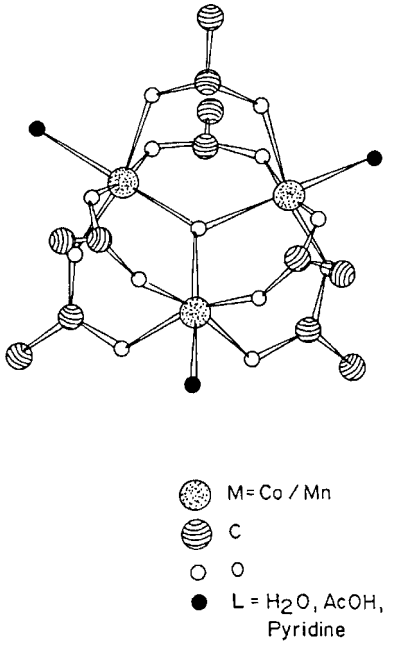

FIG. 1. Structure of μ_3-oxo-bridged Co/Mn cluster complex.

S. D. Fine Chemicals, India. PX, procured from Aldrich Co., was used as received. Zeolite-Y (H-form) was prepared from NH_4Y by calcination.

Catalyst Preparation

$[Co_3(O)(CH_3COO)_6(pyridine)_3]ClO_4(Co_3(O))$. This was prepared by a method analogous to that of Sumner and Steinmetz (17). $Co(CH_3COO)_2 \cdot 4H_2O$ (1.25 g) was taken in a solution of glacial acetic acid (12.5 ml) and pyridine (0.4 ml) and warmed at 323 K while stirring until all the solid was dissolved. The purple-colored solution was then cooled to 298 K, and a freshly prepared peracetic acid (obtained from the addition of 0.4 g of glacial acetic acid and 0.7 g of 30% H_2O_2) was added dropwise over a period of 30 min while stirring. During the addition of peracetic acid, the color of the solution changed to dark brown. Then, 3 ml of water was added and refluxed for 1 h at 353 K. A solution of $NaClO_4$ (0.4 g) dissolved in 20 ml of distilled water was added to the cooled reaction mixture. Good-quality microcrystals of $Co_3(O)$ were obtained from the solution kept at 278 K. Elemental analysis was calculated as follows: C, 35.66%; H, 3.69%; N, 4.99%. Elements found were C, 35.07%; H, 3.74%; N, 4.85%.

$[Mn_3(O)(CH_3COO)_6(pyridine)_3]ClO_4(Mn_3(O))$. This complex was prepared as per the method of Vincent *et al.* (18). $Mn(CH_3COO)_2 \cdot 4H_2O$ (2.5 g) was dissolved in a solvent mixture composed of ethanol (20 ml), glacial acetic acid (12 ml), and pyridine (3 ml). The resulting solution was stirred while adding N-*n*-Bu_4MnO_4 (1.14 g) dissolved in 10 ml ethanol, in small proportions, over a period of 45 min. The resultant brown solution was stirred for 30 min. Then, 0.695 g of $NaClO_4$ was added and the stirring was continued for further 15 min. A brown crystalline product ($Mn_3(O)$) was obtained overnight on slow evaporation at 295 K. This was filtered, washed with ethanol, and dried in vacuum. Elemental analysis was calculated as follows: C, 37.12%; H, 3.99%; N, 4.56%. Elements found were C, 37.04%; H, 4.28%; N, 4.48%.

$CoMn_2(O)(CH_3COO)_6(pyridine)_3(CoMn_2(O))$. Manganic acetate (2.7 g) was taken in a solution composed of ethanol (25 ml) and glacial acetic acid (4.2 ml) and stirred for 10 min until all the manganic acetate dissolved. To this brown solution $Co(CH_3COO)_2 \cdot 4H_2O$ (2.5 g) dissolved in hot pyridine (4 g) was added while being stirred continuously. The solution was allowed to stand at 298 K, from which shiny black crystals of μ_3-oxo-bridged Co/Mn mixed cluster, $CoMn_2(O)$, were obtained. The crystals were filtered, washed with ethanol, and dried in vacuum. Elemental analysis was calculated as follows: C, 43.39%; H, 4.41%; N, 1.87%. Elements found were C, 43.53%; H, 4.77%; N, 1.87%.

Mn–Y and Co–Y. $Mn(CH_3COOH)_2 \cdot 4H_2O$ (4.3 g) dissolved in 50 ml of distilled water was added slowly to a suspension of 7 g of zeolite-HY in 50 ml of water. The slurry was stirred for 4–5 h, at 333 K and then allowed to stand overnight at 298 K. The solid Mn-exchanged HY was filtered, washed with warm deionized water (about 500 ml), and dried at 393 K. Co–Y was prepared in a similar manner except that $Co(CH_3COOH)_2 \cdot 4H_2O$ (4.3 g) was used in place of $Mn(CH_3COOH)_2 \cdot 4H_2O$. The Mn content in Mn–Y and Co content in Co–Y were estimated to be 3.08 and 10.21 wt%, respectively.

CoMn–Y. In the preparation of CoMn–Y, 1.43 g of $Co(CH_3COOH)_2 \cdot 4H_2O$ and 4.3 g of $Mn(CH_3COOH)_2 \cdot 4H_2O$ were used, for 7 g of zeolite HY, for ion exchanging. Zeolite-HY was initially exchanged with Mn ions, as described above. The Mn–Y thus formed was then used for further exchange with Co ions to form finally CoMn–Y. The Co and Mn contents in CoMn–Y were estimated to be 1.02 and 2.10 wt%, respectively.

The encapsulated complexes were prepared by the "flexible ligand synthesis" method (19).

$[Co_3(O)(CH_3COO)_6(pyridine)_3]$–$Y(Co_3(O)$–$Y)$. In a typical preparation of encapsulated μ_3-oxo-bridged Co cluster complex, 1.5 g of Co–Y was suspended in 15 ml of HOAc taken in a double-necked, round-bottom flask fitted with an air condenser and an inlet for air. The suspension was stirred gently for 30 min while passing air. To this was added 3 ml of pyridine dropwise with stirring for 15 min. Then 0.5 g of NaBr and 5 ml of distilled water were added and the solution was stirred for another 30 min. To this 10 ml of aqueous H_2O_2 (50%) was added dropwise and the slurry was stirred for another 2–3 h, at 298 K, while passing

air. The pink solid $Co_3(O)$–Y was filtered, washed with acetic acid until all the metal complexes adsorbed on the external surface were removed, and dried at 298 K, under vacuum. It may be mentioned that all the metal complexes and clusters of the present study are highly soluble in acetic acid. Co content in zeolite–Y was estimated to be 0.70 wt%.

$[Mn_3(O)(CH_3COO)_6(pyridine)_3]$–Y($Mn_3(O)$–Y). Encapsulated oxo-bridged Mn cluster complex, $Mn_3(O)$–Y (pale brown), was prepared in a manner similar to that of $Co_3(O)$–Y, except that Mn–Y was used in place of Co–Y. Manganese content in zeolite–Y was estimated to be 1.38 wt%.

$[CoMn_2(O)(CH_3COO)_6(pyridine)_3]$–Y($CoMn_2(O)$–Y). Encapsulated oxo-bridged mixed metal complex, $CoMn_2(O)$–Y (purple), was prepared in a manner similar to that of $Co_3(O)$–Y except that CoMn–Y was used in place of Co–Y. The amounts of Co and Mn were estimated to be 0.38 and 1.31 wt%, respectively.

Procedures

Metal compositions were estimated using inductively coupled plasma–atomic emission spectroscopy (Perkin–Elmer PE-1000) and atomic absorption spectroscopy (AAS; Varian Spectr SF-220) techniques. C, H, and N analyses of neat complexes were done on a Carlo Erba EA 1108 elemental analyzer. Powder X-ray diffractograms of neat and encapsulated metal cluster complexes were recorded on a Rigaku Miniflex X-ray diffractometer with a CuKα radiation. Thermogravimetric and differential thermal analyses were performed on a Setaram TG-DTA 92 automatic derivatograph. Fourier transform infrared (FT-IR) spectra of neat and encapsulated solid complexes were recorded on a Shimadzu FT-COM 1 spectrophotometer as nujol mulls. Ultra violet (UV)–visible spectra in normal and diffuse reflectance modes were measured using a UV-101PC scanning spectrophotometer. X-ray photoemission spectra (XPS) were recorded on a VG Microtech Multilab ESCA 3000 spectrometer using MgKα radiation ($h\nu = 1253.6$ eV). EPR spectra were recorded in the temperature range 82–300 K, using an X-band Bruker EMX spectrometer and a BVT 3000 temperature controller. The spectra at 77 K were recorded using a quartz finger dewar (Bruker ER167 FDS-Q). Molecular modeling studies were carried out on a Silicon Graphics O_2 workstation.

To gain deeper insight into the redox properties of Co and Mn ions, cyclic voltammetry (CV) experiments were carried out using a BAS CV-50 electrochemical system on the homogeneous acetic acid solutions (0.004 M) of cobalt and manganese acetate salts, as well as on the neat cluster complexes, using a Pt-working electrode, a Pt-wire auxiliary electrode, and a saturated calomel reference electrode; 0.1 M tetraethyl ammonium perchlorate was used as a supporting electrolyte.

Catalytic Activity Studies and Product Analysis

In a typical oxidation reaction, 2 ml of PX, 38 ml of HOAc, 5.6 ml of distilled water, 0.0865 g of NaBr, and a catalyst were taken in a closed titanium-lined Parr 4833 reactor which was subsequently pressurized to 200–550 psig at 298 K with oxidant, air. The reactions were conducted at 473 K for a period of 15 min to 4 h (the pressure went up to about 880 psig at reaction temperature, for an initial pressure of 550 psig). The products of the oxidation are *para*-tolyl alcohol (A), *para*-tolyl aldehyde (B), *para*-toluic acid (C), 4-CBA (D), terephthalic acid (E), and benzoic acid (F). The liquid products A and B and unreacted PX were estimated by gas chromatography using a Shimadzu GC 14 B, SE 30 S.S. packed column. These liquid products and acetic acid were separated from the final reaction mixture by distillation. The solid products C, D, E, and F were converted into water-soluble sodium salts by means of 0.1 N NaOH and acetic acid solutions and estimated by high-performance liquid chromatography (HPLC) (Shimadzu LC-9A) using a Shimadzu C-R4A Chromatopac, C18 column. The weights of the liquid and solid products were noted for each run and mass balance was verified.

Separation and Recycle of the Solid Catalyst

The solid, encapsulated cluster catalyst was separated from the products as follows: The solid product mixture containing the encapsulated catalyst was treated with 0.1 N NaOH, until pH of $\approx$7, converting all the solid carboxylic acids into water-soluble salts. The zeolite catalyst was separated by filtration. No significant leaching was observed (chemical analysis). The catalyst retained its activity and could be reused.

RESULTS AND DISCUSSION

Physicochemical Characteristics

The chemical compositions of the metal complexes and solid catalysts are given in the experimental section.

XRD. No major changes were observed in the X-ray diffraction (XRD) patterns of zeolite HY on encapsulation of μ_3-oxo-bridged Co/Mn cluster complexes, indicating that encapsulation did not alter the framework structure of zeolite–Y. XPS data (not shown) confirm that Co is present in the trivalent oxidation state in the neat as well as the zeolite-encapsulated samples.

TGA. The thermogravimetric and differential thermogravimetric analysis (TG-DTG) profiles of different catalysts are shown in Fig. 2. The peak maximum around 480 K in the DTG of $Co_3(O)$ (Fig. 2) corresponds to loss of coordinated pyridine, and that at 549 K is due to decomposition of the acetate ligand. The weight losses in two stages

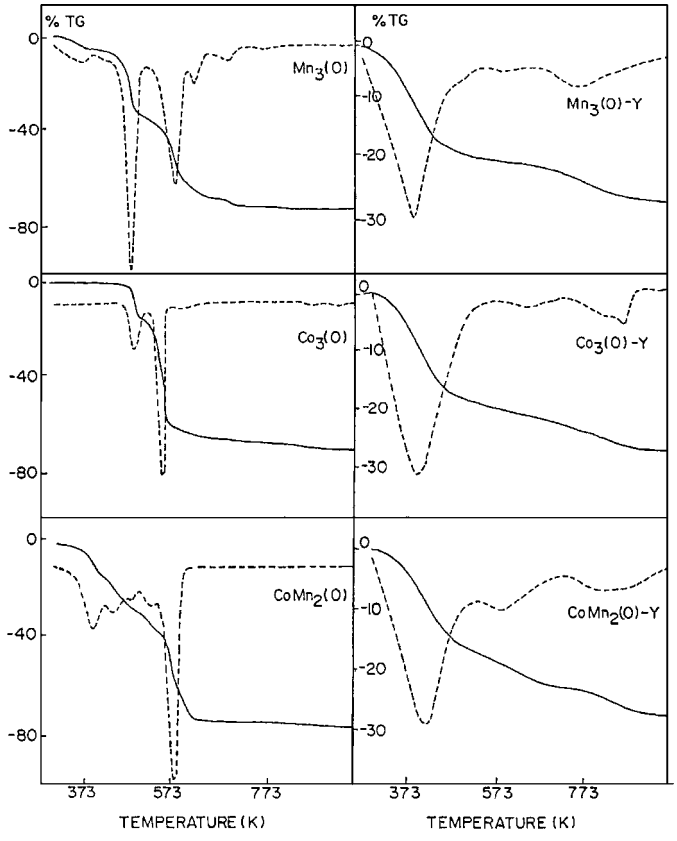

FIG. 2. TGA (—) and DTG (- - -) profiles of neat and encapsulated μ_3-oxo-bridged cluster complexes.

in the range 563–663 K correspond to decomposition of the counterion perchlorate initially into ClO and then into chlorine. The weight loss in the range 818–936 K corresponds to decomposition of secondary products like $CoCO_3$ (formed from the acetate) into cobalt oxide-type materials. In $Mn_3(O)$ cluster, the DTG peak at 388 K is due to the loss of water. Pyridine decomposition is observed at 454–495 K (peak maximum around 484 K). The decomposition of acetate in $Mn_3(O)$ occurs in the range 497–603 K, with peak maximum at 577 K. The peaks with maxima at 616 and 700 K are due to decomposition of the perchlorate ion. The weight loss with a peak maximum at around 390 K in $CoMn_2(O)$ is due to water loss. The three DTG peaks, due to loss of pyridine, in the temperature range 423–529 K, arise perhaps from differences in bond strengths of pyridine coordinated to Co and Mn ions. The decomposition of the acetate occurs at 563 K. In the case of the zeolite-Y-encapsulated catalysts, the peaks corresponding to adsorbed/bound water dominate those of acetate and pyridine ligands (Fig. 2). The DTG peaks of the latter appear as shoulders in the range 493–593 K. The broad multistep peak in the range 723–923 K is due to the decomposition of secondary carbonates (formed from the acetate) during thermal analysis.

FT-IR spectroscopy. The FT-IR bands of the zeolite framework and adsorbed water overlap those of the acetate and pyridine ligands (Fig. 3). Neat $Mn_3(O)$ and $Co_3(O)$ cluster complexes (curves a and b, respectively) show additional peaks around 1092, 1072, 1047, 1032, and 762 cm^{-1} due to the counterion (perchlorate). The μ_3-oxo-bridge in $Mn_3(O)$ shows a characteristic peak at 665 cm^{-1}. The position of this peak is sensitive to the coordinated metal ion and occurs at 692 and 685 cm^{-1} for $Co_3(O)$ and $CoMn_2(O)$, respectively (curves b and c, respectively). The spectral assignments of different bands for neat and encapsulated complexes are presented in Table 1. The COO^- vibrational modes of acetate groups shift to lower energy (i.e., toward higher wavenumbers) on encapsulation (Fig. 3 and Table 1). The separation ($\Delta\nu$) between $\nu_{as}(COO^-)$ and $\nu_s(COO^-)$ is in the range 165–212 cm^{-1}, indicative of bidentate COO^- coordination, in *syn–syn* mode, to two metal ions (20).

UV–visible spectroscopy. Acetic acid solutions of the neat complexes show an intense UV band, of ligand origin, around 254 nm and a shoulder at 280 nm (Fig. 4, curves a–c). In addition to these, a weak, partially resolved band, characteristic of a μ_3-oxo-bridge, is also observed at around 320 nm for $Mn_3(O)$ and at 355 and 345 nm for $Co_3(O)$ and $CoMn_2(O)$, respectively. The position of the latter band is sensitive to the coordinated metal ion and is attributed to oxygen ⇒ metal charge transfer transitions. This band is seen even in the diffuse reflectance UV–visible spectra of encapsulated cluster complexes (curves d–f of Fig. 4). However, due to the dilution in the zeolite matrix, it could be seen only in $Co_3(O)$–Y (curve d). The observation of these bands confirms the presence and structural integrity of these cluster complexes in the cavities of the zeolite.

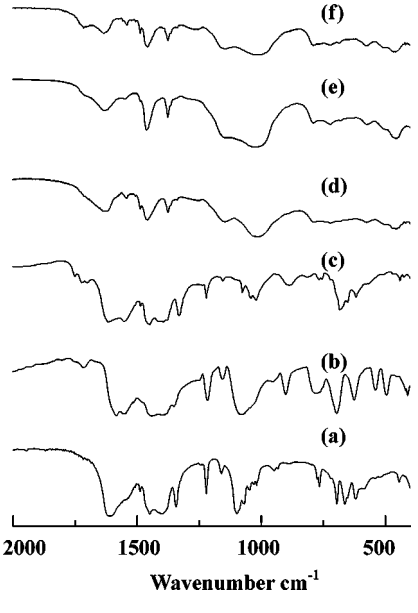

FIG. 3. FT-IR spectra (in nujol mull): (a) $Mn_3(O)$, (b) $Co_3(O)$, (c) $CoMn_2(O)$, (d) $Mn_3(O)$–Y, (e) $Co_3(O)$–Y, and (f) $CoMn_2(O)$–Y.

TABLE 1

FT-IR Assignments for Neat and Encapsulated Oxo-Bridged Metal Cluster Complexes

Assignment	$Mn_3(O)$		$Co_3(O)$		$CoMn_2(O)$	
	Neat (cm^{-1})	Encapsulated (cm^{-1})	Neat (cm^{-1})	Encapsulated (cm^{-1})	Neat (cm^{-1})	Encapsulated (cm^{-1})
Asymmetric and symmetric C–H stretch	2924	2924	2924	2924	2924	2924
COO^- asymmetric stretch	1605	1624	1609	1635	1616	1635
COO^- symmetric stretch	1404	1458	1402	1463	1404	1458
CH bending (CH_3)	1456	1489	1452	1463	1448	1489
	1342	1340	1352		1350	1340
COO^- deformation	617	—[a]	623	—[a]	619	—[a]
C=N stretch (Py)	1558	1545	1558	1550	1553	1545

[a] Masked by zeolite bands.

EPR spectroscopy. The neat $Mn_3(O)$ cluster complex shows a broad, isotropic signal at $g = 2.01$ with a peak-to-peak linewidth (ΔH_{pp}) of 500 G. The isotropic nature is due to the small zero-field interaction in the cluster complex. The position and ΔH_{pp} of the signal are invariant to temperature, in the range 77–298 K. However, the intensity of the EPR signal, determined from the double integration method, increases with decreasing temperature (Fig. 5, curve a), indicating that the antiferromagnetic interaction (among Mn(III) ions, resulting in an $s = 2$ ground state) is rather weak in this complex. This is the first report on the EPR characteristics of this cluster complex. Its magnetic behavior was reported by Vincent *et al.* (18), who found the exchange coupling constant (J) to be $-10.2\ cm^{-1}$. Our EPR results are in agreement with the small J values reported by them. Polycrystals of the neat $Co_3(O)$ cluster complex also show isotropic signals at 300 K but at a higher g value (2.259) and with a larger linewidth (1075 G). Unlike $Mn_3(O)$, the variation with temperature of the signal intensity, g value, and linewidth (Fig. 5, curves b–d, respectively) of $Co_3(O)$ clusters indicate strong antiferromagnetic interaction. The Curie temperature is around 130 K for the $Co_3(O)$ cluster. It is below 77 K for Mn_3O. The $CoMn_2(O)$, on the other hand, is EPR-silent throughout the temperature range.

The encapsulated $Mn_3(O)$ cluster complex ($Mn_3(O)$–Y) shows a broad EPR signal at $g = 2.012$ with barely resolved manganese hyperfine features superimposed on the broad signal (Fig. 6, curve a). Encapsulated $Co_3(O)$ complexes also exhibit a broad signal at $g = 2.210$ (Fig. 6, curve b), the intensity of which decreases at low temperatures and disappears totally at 77 K. The variation of the signal intensity in the neat and encapsulated $Co_3(O)$ complexes is similar and indicates strong intramolecular antiferromagnetic interactions. $Co_3(O)$–Y samples also revealed trace amounts of a Mn(II) ion impurity present in the parent zeolite sample (marked by an asterisk in Fig. 6). Mixed metal clusters encapsulated in zeolite–Y showed (curve c) a Mn-like spectrum at $g = 2.026$. A shift in g value from 2.012, typical of a $Mn_3(O)$–Y cluster, is due to the presence

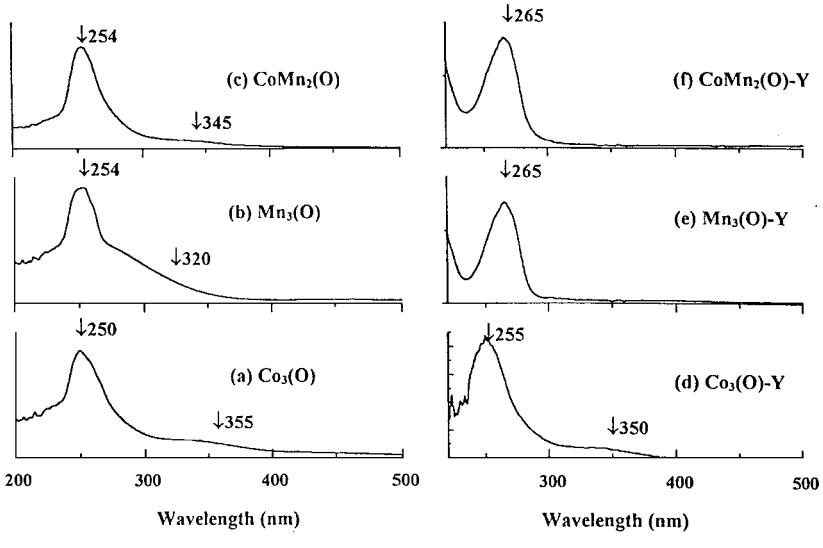

FIG. 4. UV–visible (for neat) and diffuse reflectance UV–visible (for encapsulated) spectra of μ_3-oxo-bridged cluster complexes: (a) $Co_3(O)$, (b) $Mn_3(O)$, (c) $CoMn_2(O)$, (d) $Co_3(O)$–Y, (e) $Mn_3(O)$–Y, and (f) $CoMn_2(O)$–Y.

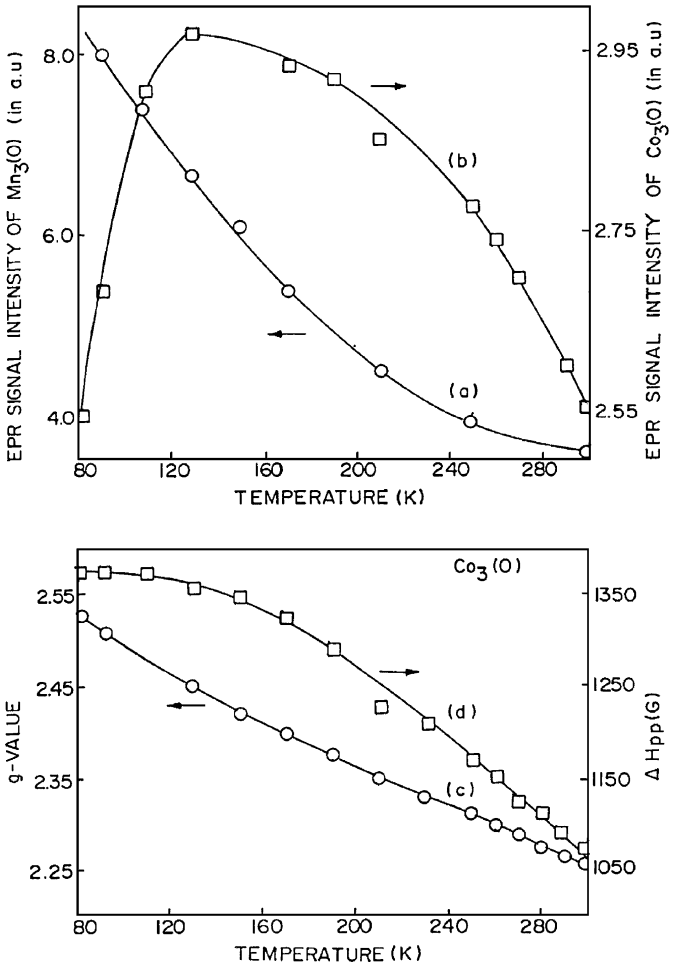

FIG. 5. Variation of EPR signal intensity with temperature for (a) neat $Mn_3(O)$ and (b) $Co_3(O)$ cluster catalysts. Variation of (c) g value and (d) linewidth (ΔH_{pp}) with temperature for neat $Co_3(O)$ cluster complex.

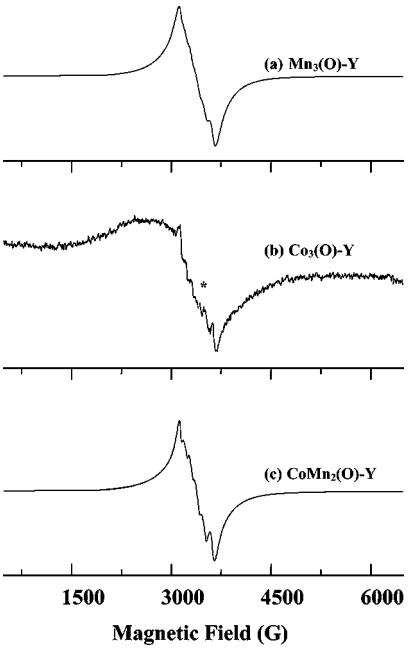

FIG. 6. X-band EPR spectra of encapsulated μ_3-oxo-bridged Co/Mn cluster complexes at 298 K: (a) $Mn_3(O)$–Y, (b) $Co_3(O)$–Y. The broad signal is due to the encapsulated cobalt cluster (the six sharp signals marked by an asterisk are due to Mn impurity). (c) $CoMn_2(O)$–Y.

of Co in the trinuclear unit, confirming the structural integrity of the $CoMn_2(O)$ cluster in zeolite–Y, a conclusion also reached from the FT-IR and UV–visible spectral data.

Stability of Cluster Complexes under Reaction Conditions

Figure 7 shows the EPR spectra of the $Mn_3(O)$ complex and NaBr dissolved in acetic acid and heated in air (550 psig) to 473 K for 1 h (curves a–c of Fig. 7). The spectral features reveal the structural stability of these oxo-bridged cluster complexes under typical reaction conditions. Heating a mixture of $Mn(CH_3COO)_2 \cdot 4H_2O$ solution in acetic acid, NaBr, and air (550 psig), in fact, converts the linear manganese acetate into a trimeric $Mn_3(O)$ cluster complex (compare curves a and d of Fig. 7). This observation also confirms that the Mn cluster complexes are formed during the course of the reaction even with the conventional catalyst system (Co/Mn/Br^-/acetic acid), as postulated by us in our earlier publication (16).

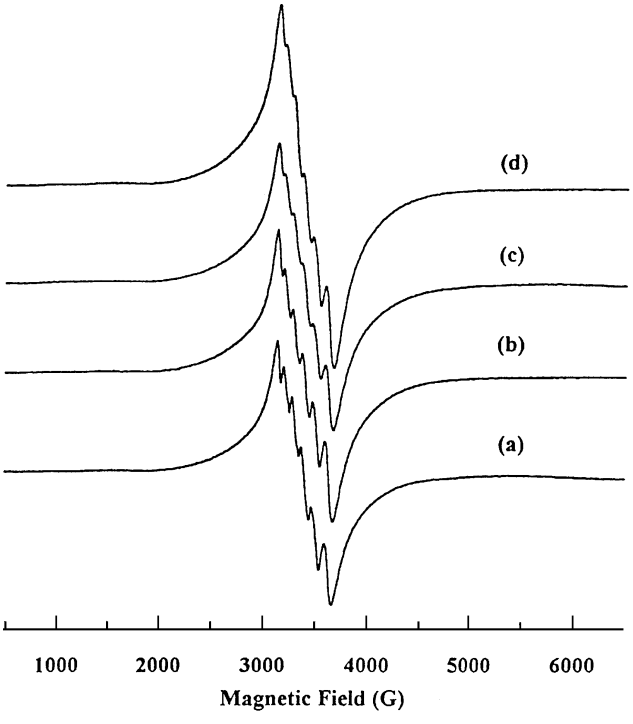

FIG. 7. EPR spectra (at 82 K) of $Mn_3(O)$: (a) $Mn_3(O)$ + HOAc + NaBr; (b) $Mn_3(O)$ + HOAc + NaBr after 1 h at 473 K; (c) $Mn_3(O)$ + HOAc + NaBr after 1 h at 473 K and 550 psig air; and (d) $Mn(CH_3COO)_2 \cdot 4H_2O$ + HOAc + NaBr after 1 h at 473 K and 550 psig air.

TABLE 2

Effect of Solvent and Halide Ion on the Oxidation of *para*-Xylene over Co/Mn Catalysts in Homogeneous Medium Reaction Conditions[a]

Run no.	Catalyst (mmol)	Solvent/halide ion	Conversion (wt%)	TON[b]	Product distribution (wt%)[c]					
					A	B	C	D	E	F
1	$Co(OAc)_2$(0.43) + $Mn(OAc)_2$(0.14)	1,4-Dioxane, Br^-	35.1	11	11.2	88.5	0.3			
2	$Co(OAc)_2$(0.43) + $Mn(OAc)_2$(0.14)	AcOH, Cl^-	18.0	6	1.7	74.7	23.6			
3	$Co(OAc)_2$(0.43) + $Mn(OAc)_2$(0.14)	AcOH, Br^-	100	32	0	0	0.9	0.1	97.7	1.3
4	$Co_3(O)$ (0.041)	1,4-Dioxane, Br^-	17.3	78	23.8	76.2	0			
5	$Mn_3(O)$(0.039)	1,4-Dioxane, Br^-	46.0	216	14.0	84.6	1.4			
6	$CoMn_2(O)$(0.041)	1,4-Dioxane, Br^-	23.5	106	24.0	74.8	1.2			
7	$Co(OAc)_2$(0.43) + $Mn(OAc)_2$(0.14)	AcOH[d]	2.3	1	6.8	52.5	40.7			
8	$Co_3(O)$ (0.041)	AcOH[d]	4.3	20	0	63.7	36.3			
9	$Mn_3(O)$(0.039)	AcOH[d]	0.5	2	0	70.9	29.1			
10	$CoMn_2(O)$(0.041)	AcOH[d]	7.5	34	1.6	75.2	23.3			

[a] *para*-Xylene (2 ml) + NaBr (0.0836 g) + H_2O (5.6 ml) + HOAc (38 ml); oxidant, air; reaction time, 45 min; temperature, 473 K; pressure, 550 psig.
[b] Turnover number (TON), mole of *para*-xylene converted per mole of metal catalyst.
[c] Products: A, *p*-tolyl alcohol; B, *p*-tolyl aldehyde; C, *p*-toluic acid; D, 4-carboxybenzaldehyde; E, terephthalic acid; and F, benzoic acid. Liquid products A and B were estimated using gas chromatography. Products C to F were estimated using HPLC.
[d] Reaction without any halide ion.

Selective Oxidation of PX

In the commercial process for the selective oxidation of PX to TA, in addition to complete conversion of the PX, it is also essential to get as high a selectivity for TA as possible. Particularly, it is desirable to suppress or eliminate the 4-CBA impurity. In current practice, 4-CBA occurs to the extent of 0.1–0.5% in the crude product. In the following sections we report the activities of the neat and zeolite-encapsulated cluster catalysts. The catalytic data are presented in Tables 2–5. The reaction did not proceed to any significant extent in the absence of catalyst.

Effect of solvent and halide ion. When the reactions are carried out with NaCl in place of NaBr (Table 2), the conversions are markedly lower (compare runs 2 and 3). The conversions are also low in the absence of the halide ion (runs 7–10), or when 1,4-dioxane is used in place of acetic acid (runs 1 and 4–6). Both acetic acid and the bromide ion are essential for high activity and selectivity.

TABLE 3

Oxidation of *para*-Xylene over $Co(CH_3COO)_3 \cdot 4H_2O$ and $Mn(CH_3COO)_2 \cdot 4H_2O$ Salts in Homogeneous Medium Reaction Conditions[a]

Run no.	Catalyst (mmol)[b]	Pressure (psig)	Conv. (wt%)	TON[c]	Product distribution (wt%)[d]					
					A	B	C	D	E	F
1	Co(0.43)	200	84.7	36	1.6	39.4	21.4	8.8	28.4	0.3
2	Co(0.43) + Mn(0.14)	200	83.4	27	0	40.3	23.0	6.4	30.1	0.2
3	Co(0.28) + Mn(0.28)	200	89.1	30	0	44.4	24.6	10.4	20.1	0.6
4	Co(0.14) + Mn(0.44)	200	87.4	28	0	43.6	25.3	13.3	17.3	0.5
5	Mn(0.44)	200	89.1	38	0	44.0	24.7	12.9	17.2	1.2
6	Co(0.43)	350	100	43	0	0	14.1	2.2	83.6	0.1
7	Co(0.43) + Mn(0.14)	350	100	32	0	0	0.8	0.01	98.8	0.4
8	Co(0.28) + Mn(0.28)	350	100	33	0	0	1.6	0.1	98.2	0.1
9	Co(0.14) + Mn(0.44)	350	100	32	0	0	5.0	0.2	92.8	2.0
10	Mn(0.44)	350	100	42	0	0	23.7	5.0	70.9	0.4
11	Co(0.43) + Mn(0.14)	550	100	32	0	0	0.7	1.4	96.9	0.01
12	Co(0.28) + Mn(0.28)	550	100	33	0	0	0.36	0.03	99.6	0.01
13	Co(0.14) + Mn(0.44)	550	100	32	0	0	0.44	0.05	99.5	0.01
14	Mn(0.44)	550	99	42	0	0	7.3	1.0	91.7	0.02

[a] Reaction conditions are the same as in Table 2. Reaction time, 2 h; temperature, 473 K.
[b] Sources of Co and Mn are $Co(CH_3COO)_2 \cdot 4H_2O$ and $Mn(CH_3COO)_2 \cdot 4H_2O$, respectively.
[c] Turnover number (TON), mole of *para*-xylene converted per mole of metal catalyst.
[d] Products are the same as in the Table 2.

TABLE 4

Catalytic Activity of Neat Co/Mn Cluster Catalysts in the Selective Oxidation of *para*-Xylene in Homogeneous Medium: Effect of Pressure and Reaction Time[a]

Run no.	Catalyst (mmol)	Pressure (psig)	Reaction time (min)	Conversion (wt%)	TON[b]	Product distribution (wt%)[c]					
						A	B	C	D	E	F
1	$Co_3(O)$(0.041)	550	15	67.7	307	0.5	26.5	20.1	46.7	5.3	0.9
2			30	75.6	343	0.5	33.6	25.3	33.3	6.4	0.9
3			45	86.7	393	0	42.5	26.0	11.7	19.5	0.3
4	$Mn_3(O)$(0.039)	550	15	79.4	373	0	37.6	27.4	22.9	11.2	0.9
5			30	64.5	303	0	22.5	26.1	10.3	40.8	0.3
6			45	100	470	0	0	27.0	8.0	64.9	0.1
7			120	100	470	0	0	1.6	0.1	98.2	0.1
8	$CoMn_2(O)$(0.041)	550	15	100	449	0	0	4.0	0.3	95.7	0
9			30	100	449	0	0	6.1	0.9	93.0	0
10			45	100	449	0	0	4.7	0.7	94.6	0
11			60	100	449	0	0	1.8	0.4	97.8	0
12			120	100	449	0	0	0.8	0.1	99.0	0.1

[a] Reaction conditions are the same as in Table 2. Reaction temperature, 473 K.
[b] Turnover number (TON), mole of *para*-xylene converted per mole of metal catalyst.
[c] Products are the same as in Table 2.

PX oxidation over cobalt and manganese acetate salts. When mixtures of the cobalt and manganese acetates are used, the clusters are formed in about 15 min at higher pressures (350–550 psig) and temperatures (above 473 K) compared to about 4 h at atmospheric pressure and 363 K. The combination of cobalt and manganese acetates in millimole ratios of 3 : 1, 1 : 3, and 1 : 1 yield cluster complexes of the type $Co_2Mn(O)$, $CoMn_2(O)$, and a mixture of $Co_2Mn(O)$ and $CoMn_2(O)$, respectively (16). Both conversion and selectivity are higher when Co and Mn are present together (Table 3). Complete conversion of PX and >95 wt% selectivity to TA are obtained at 550 psig and 473 K (Table 3, runs 7, 8, 11–14).

PX oxidation over neat cluster catalysts. At 473 K and a pressure of 550 psig, 100% PX conversion and >98 wt% TA selectivity is obtained with the cluster catalysts ($Mn_3(O)$ and $CoMn_2(O)$) (runs 7 and 12 of Table 4). Complete conversion of PX is achieved within 15 min with $CoMn_2(O)$ (run 8). However, TA selectivity improves when reactions are continued for a longer time (runs 8–12). $Co_3(O)$ exhibits low PX conversions and TA selectivity. $Mn_3(O)$, on the other hand, yields 100% PX conversion and high TA selectivity at longer reaction times (run 7). It may be noted that the heteronuclear cluster catalyst $CoMn_2(O)$ is more active and yields higher TA selectivity than the homonuclear $Co_3(O)$ and $Mn_3(O)$. The concentration of 4-CBA is also, in general, less with the former.

PX oxidation over solid catalysts. When the complexes are encapsulated in zeolite–Y, complete conversions are achieved only at longer reaction times (Table 5), perhaps

TABLE 5

Catalytic Activity of Solid Catalysts: μ_3-Oxo-Bridged Co/Mn Clusters Encapsulated in Zeolite–Y[a]

Run no.	Catalyst (g · mmol of metal)	Time (min)	Conversion (wt%)	TON[b]	Product distribution (wt%)[c]					
					A	B	C	D	E	F
1	$Mn_3(O)$–Y (0.075)	60	74.8	183	0	33.1	47.3	8.1	10.4	1.1
2		150	80.4	197	0	37.8	30.8	1.7	29.7	0
3		240	99.9	245	0	0	20.1	0.7	79.2	0
4	$Co_3(O)$–Y (0.036)	60	65.6	341	13.4	18.4	13.0	37.5	15.2	2.5
5		150	72.0	374	10.5	14.0	10.7	39.8	20.7	4.3
6	$CoMn_2(O)$–Y (0.09)	60	74.4	151	0	0	6.4	0.8	92.8	0.1
7		150	100	203	0	0	1.1	<0.01	98.9	0
8		240	100	203	0	0	0.6	0.01	99.4	0

[a] Reaction conditions are the same as in Table 2. Catalyst, 0.2995 g; temperature, 473 K; and pressure, 550 psig.
[b] Turnover number (TON), mole of *para*-xylene converted per mole of metal catalyst.
[c] Products are the same as in Table 2.

TABLE 6

Cyclic Voltametric Data of Neat μ_3-Oxo-Brideged Co/Mn Cluster Complexes

Complex	Redox couple	$E_{1/2}$ (in V)[a]	ΔE (in V)[b]
$Co(CH_3COO)_2 \cdot 4H_2O$	A: Co^{III}/Co^{II}	+0.75	0.21
$Mn(CH_3COO)_2 \cdot 4H_2O$	A: Mn^{III}/Mn^{II}	+0.75	0.30
$Co_3(O)$	A: $Co_3^{III}(O)/Co^{II}Co_2^{III}(O)$	+0.69	0.22
$CoMn_2(O)$	A: $Co^{III}Mn_2^{III}(O)/Co^{II}Mn_2^{III}(O)$	+0.56	0.04
	B: $Co^{III}Mn^{IV}Mn^{III}(O)/Co^{III}Mn_2^{III}(O)$	+0.93	0.05

[a] $E_{1/2}$, Half-wave potential with reference to saturated calomel electrode.
[b] ΔE, separation between the cathodic and anodic peaks of the redox couple.

due to diffusional limitations in the zeolite. Easy separability and reusability (see Experimental section) are major advantages of the solid catalysts. Another interesting feature with the encapsulated $CoMn_2(O)$ cluster catalyst (run 8) is the very low concentration of the 4-CBA impurity (around 0.01%). It may be noted that the activity and selectivity of both the neat and encapsulated cluster complexes follow the trend $CoMn_2(O) > Mn_3(O) > Co_3(O)$, confirming the superiority of the heteronuclear complexes.

Catalyst Leaching Tests

The molecular dimensions of the $M_3(O)$ (M = Co, Mn) cluster is about 10.8 Å. It can be accommodated in the supercages of zeolite–Y (~12 Å). The cluster is, however, larger than the openings of the windows of the zeolite's supercage, and after formation it is, hence, locked inside the supercage, making its loss during the reaction difficult. Leaching of metal ions from the solid catalyst at the end of the reaction was investigated by AAS and EPR spectroscopic techniques. While AAS did not reveal any leaching of metal ions, EPR estimated that about 0.5% of the encapsulated manganese in the solid catalyst was leached into solution (about 50 ppm of Mn in solution). This amount cannot account for the observed catalytic activity. Catalytic runs with this trace amounts of metal ions in solution exhibited low PX conversions (28 wt%) with *para*-tolyl alcohol (A) and *para*-tolyl aldehyde (B) as products; TA was not detected.

μ_3-Oxo-Bridged Co/Mn Cluster Complexes and Mechanism of PX Oxidation

Role of bromide. During the reaction, Co(III) oxidizes Mn(II) to Mn(III) ions, being itself reduced to Co(II). The Mn(III) ion, in turn, abstracts an electron from the bromide ion to form a bromine atom. The bromine atom subsequently abstracts a H-atom from the $-CH_3$ group (forming HBr) and initiates the oxidation reaction. A similar abstraction of an electron from the chloride ion by Mn(III) ions to form chlorine atom (and Mn(II)) is not favorable because the $E_{1/2}$ of the Mn(III)/Mn(II) couple (1.2 V) is smaller than that of the $Cl^{\cdot}/Cl^{-}$ couple (1.36 V). The redox potentials of cobalt, manganese, bromide, and chloride ions against an

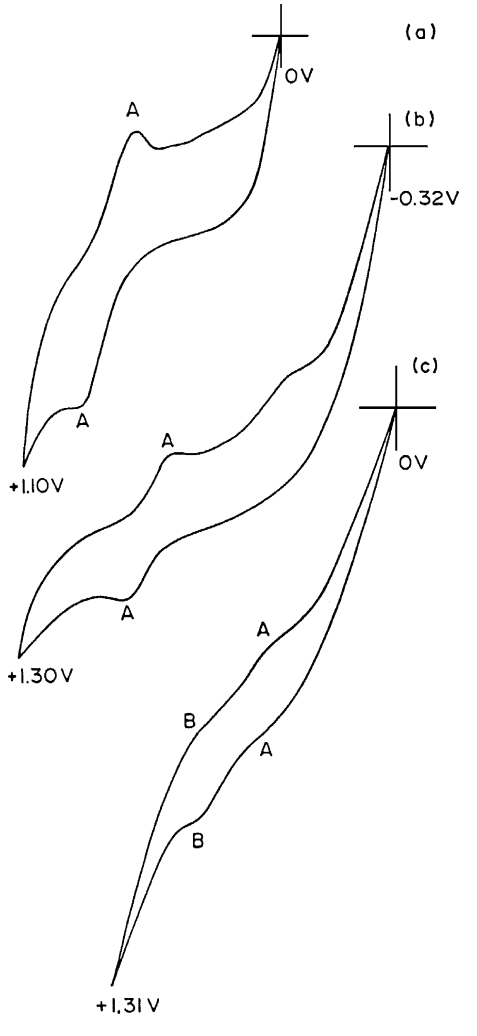

FIG. 8. Cyclic voltammograms of (a) $Co(CH_3COO)_2 \cdot 4H_2O$, (b) $Co_3(O)$, and (c) $CoMn_2(O)$. Redox couples A and B are indicated.

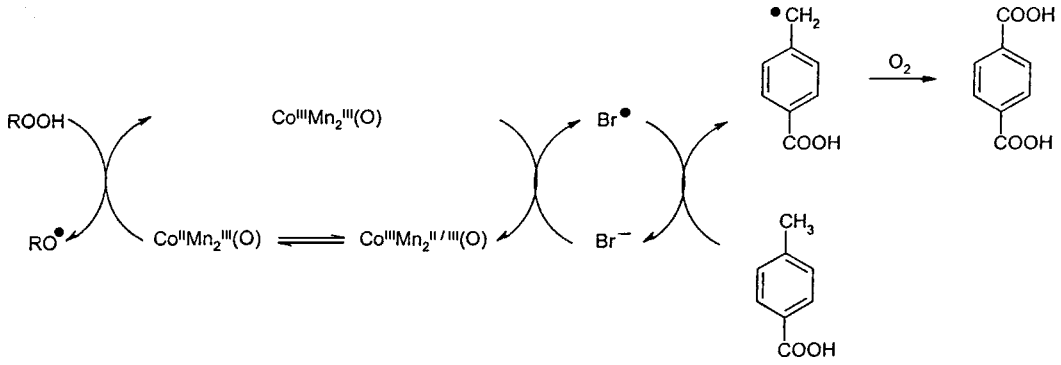

FIG. 9. Catalytic oxidation of *para*-toluic acid over $CoMn_2(O)$–Y.

NH electrode are given as (21).

$$\begin{aligned} Co(III) + e^- &\leftrightarrow Co(II) \quad (E_{1/2} = 1.92\,V)\\ Mn(II) &\leftrightarrow Mn(III) + e^- \quad (E_{1/2} = 1.2\,V)\\ Br^- &\leftrightarrow Br^{\cdot} + e^- \quad (E_{1/2} = 1.06\,V)\\ Cl^- &\leftrightarrow Cl^{\cdot} + e^- \quad (E_{1/2} = 1.36\,V). \end{aligned}$$

Chlorine atoms are also less stable than bromine and readily form chlorine molecules. The unfavorable redox couple as well as the low concentration of chlorine atoms in solution are responsible for the low conversions observed with chloride ions (Table 2). Bromide ions are, hence, the promoters of choice.

Role of the cluster complexes. The CV data of cobalt and manganese acetates and $Co_3(O)$ and $CoMn_2(O)$ are presented in Table 6. Figure 8 shows the CV of cobalt acetate, $Co_3(O)$ and $CoMn_2(O)$ (curves a–c, respectively). The redox couple A (Fig. 8) is due to changes in the oxidation state of Co (between +2 and +3). $CoMn_2(O)$ (curve c) shows an additional redox couple (B) due to $Mn^{III} \leftrightarrow Mn^{IV}$ transitions of one of the two Mn ions in $CoMn_2(O)$. The $E_{1/2}$ value for couple A is lower for $CoMn_2(O)$ (+0.56 V) compared to $Co_3(O)$ (+0.69 V) and cobalt and manganese acetates (+0.75 V), respectively (Table 6). Lower $E_{1/2}$ values are indicative of greater ease of electron transfer. The redox couples of $CoMn_2(O)$ are reversible, while those of the others are quasireversible (note the smaller ΔE values for $CoMn_2(O)$ (0.04 V) compared to $Co_3(O)$ (0.22 V), cobalt acetate (0.21 V), and manganese acetate (0.30 V); Table 6). The low $E_{1/2}$ and ΔE values indicative of more facile $Co^{II} \leftrightarrow Co^{III}$ transitions in $CoMn_2(O)$ are, perhaps, responsible for its higher catalytic activity.

The aerial oxidation of PX by a Co/Mn/Br^- catalyst system follows a free radical chain mechanism (1). The mechanism of the oxidation reaction is believed (1) to begin with H-atom abstraction from the methyl group by bromine atoms (forming HBr). The resultant benzyl radical adds to O_2 and proceeds through the hydroperoxide (22) to *para*-tolyl alcohol (A), *para*-tolyl aldehyde (B), and *para*-toluic acid (C). H-atom abstraction from the methyl group in *para*-toluic acid (C) generates a secondary benzyl radical, which follows the same pathway to yield, eventually, TA (E). The former reaction (oxidation of PX to *para*-toluic acid) is easier, and even mononuclear Co or Mn complexes accomplish this significantly (16, 23). Further oxidation of *para*-toluic acid to TA, however, is difficult and only the catalyst system Co/Mn/Br^-, in HOAc, at high pressure and temperature, achieves 100% conversion of PX with >95% selectivity to TA. The reduction in ring electron density (in going from PX to *para*-toluic acid) makes H-abstraction from methyl group of *para*-toluic acid about 4.9 times more difficult. Monomeric complexes cannot abstract H-atoms from *para*-toluic acid; μ_3-oxo-bridged heteronuclear Co/Mn clusters ($CoMn_2(O)$) are capable of accelerating the latter reaction step. A tentative reaction mechanism for oxidation by μ_3-oxo-bridged cluster complexes is shown in Fig. 9. It is interesting to note that such oxo- and acetato-bridged Fe, Cu, and Mn complexes are active sites in many oxygenase, oxidase and catalase enzymes (24–27). Cluster complexes exhibit labile intramolecular electron and spin transfer. This unique property and the basic nature of the μ_3-oxo-bridges account, perhaps, for their superior performance in the selective oxidation of PX.

CONCLUSIONS

μ_3-Oxo-bridged Co/Mn acetate cluster complexes, both in the neat state and when encapsulated in the supercages of zeolite-Y, are efficient catalysts for the selective oxidation of PX to TA. The more facile redox behavior of Co between +2 and +3 oxidation states in $CoMn_2(O)$ compared to the homonuclear complexes is responsible for the greater catalytic activity of the former. The zeolite-based heterogeneous catalysts, in addition to possessing all the superior activity and selectivity characteristics of the homogeneous catalysts, have the advantages of easy separation and reuse. The catalyst is stable at reaction conditions and there is negligible leaching of metal ions into the reaction medium. To our knowledge, this is the first solid catalyst

reported that is both highly active and selective in oxidation of *para*-xylene to terephthalic acid.

ACKNOWLEDGMENTS

The authors thank Ms. N. E. Jacob for the help in thermal analysis and Prof. Subhash Padhye and Mr. Nitin Gokhale for electrochemical studies.

REFERENCES

1. Partenheimer, W., *Catal. Today* **23**, 69 (1995).
2. Sheldon, R. A., and Van Santen, R. A. (Eds.), "Catalytic Oxidation: Principles and Applications." World Scientific, Singapore, 1995.
3. Sheldon, R. A., *in* "The Activation of Dioxygen and Homogeneous Catalytic Oxidation" (D. H. R. Barton, A. E. Martell, and D. T. Sawyer, Eds.), p. 9. Plenum, New York, 1993.
4. Sheldon, R. A., *in* "Dioxygen Activation and Homogeneous Catalytic Oxidation" (L. I. Simandi, Ed.), Vol. 66, p. 573. Elsevier, Amsterdam, 1991.
5. Parshall, G. W., and Ittel, S. D., "Homogeneous Catalysis." Wiley-Interscience, New York, 1992.
6. Saffer, A., and Barker, R. S., U.S. Patent 2,833,816 (1958).
7. PCT Int. Appl. WO 9,931,038 (24 June 1999).
8. Partenheimer, W., and Schammel, W. P., U.S. Patent 4,786,753 (1988).
9. Broeker, J. L., Partenheimer, W., and Rosen, B. I., U.S. Patent 5,453,538 (1995).
10. Hutchings, G. J., *Chem. Commun.* 301 (1999).
11. Sabater, M. J., Corma, A., Domenech, A., Fornés, V., and Garcia, H., *Chem. Commun.* 1285 (1997).
12. Ogunwumi, S. B., and Bein, T., *Chem. Commun.* 901 (1997).
13. Parton, R. F., Bezoukheanova, C. P., Grobet, J., Grobet, P. J., and Jacobs, P. A., *Stud. Surf. Sci. Catal.* **83**, 371 (1994).
14. Deshpande, S., Srinivas, D., and Ratnasamy, P., *J. Catal.* **188**, 261 (1999).
15. Chavan, S., Srinivas, D., and Ratnasamy, P., *Top. Catal.* **11/12**, 359 (2000).
16. Chavan, S. A., Halligudi, S. B., Srinivas, D., and Ratnasamy, P., *J. Mol. Catal.* **161**, 49 (2000).
17. Sumner, C. E., Jr., and Steinmetz, G. R., *J. Am. Chem. Soc.* **107**, 6124 (1985).
18. Vincent, J. B., Chang, H.-R., Folting, K., Huffman, J. C., Christou, G., and Hendrickson, D. N., *J. Am. Chem. Soc.* **109**, 5704 (1987).
19. Balkus, K. J., Jr., and Gabrielov, A. G., *J. Inclusion Phenom. Mol. Recognit. Chem.* **21**, 159 (1995).
20. Mehrotra, R. C., and Bohra, R., "Metal Carboxylates." Academic Press, New York, 1983.
21. Douglas, B. E., McDaniel, D. H., and Alexander, J. J., "Concepts and Models in Inorganic Chemistry." Wiley, New York, 1994.
22. Metelski, P. D., Adamian, V. A., and Espenson, J. H., *Inorg. Chem.* **39**, 2434 (2000).
23. Jacob, C. R., Varkey, S. P., and Ratnasamy, P., *Appl. Catal. A* **182**, 91 (1999).
24. Andersson, K. K., and Gräslund, A., *Adv. Inorg. Chem.* **43**, 359 (1995).
25. Siegbahn, P. E. M., and Crabtree, R. H., *in* "Metal-Oxo and Metal-Peroxo Species in Catalytic Oxidations in Structure and Bonding" (B. Meunier, Ed.), Vol. 97, p. 125. Springer-Verlag, Berlin, 2000.
26. Beyer, W. F., and Fridovich, I., *Biochemistry* **24**, 6460 (1985).
27. Law, N. A., Caudu, M. T., and Pecoraro, V. L., *Adv. Inorg. Chem.* **46**, 305 (1999).